ChemPubSoc Europe

DOI: 10.1002/chem.201503136

CHEMISTRY A European Journal Full Paper

Heterogeneous Catalysis

Effects of Coke Deposits on the Catalytic Performance of Large Zeolite H-ZSM-5 Crystals during Alcohol-to-Hydrocarbon Reactions as Investigated by a Combination of Optical Spectroscopy and Microscopy

Emily C. Nordvang,[b] Elena Borodina,[a] Javier Ruiz-Martínez,[a] Rasmus Fehrmann,[b] and Bert M. Weckhuysen*[a]

Abstract: The catalytic activity of large zeolite H-ZSM-5 crystals in methanol (MTO) and ethanol-to-olefins (ETO) conversions was investigated and, using operando UV/Vis measurements, the catalytic activity and deactivation was correlated with the formation of coke. These findings were related to in situ single crystal UV/Vis and confocal fluorescence microspectroscopy, allowing the observation of the spatiotemporal formation of intermediates and coke species during the MTO and ETO conversions. It was observed that rapid deactivation at elevated temperatures was due to the fast formation of aromatics at the periphery of the H-ZSM-5 crystals, which are transformed into more poly-aromatic coke species at the external surface, preventing the diffusion of reactants and products into and out of the H-ZSM-5 crystal. Furthermore, we were able to correlate the operando UV/Vis spectroscopy results observed during catalytic testing with the single crystal in situ results.

Introduction

Methanol-to-hydrocarbons (MTH) processes have been extensively researched both in industry and academia, originally as alternative sources for gasoline from natural gas, however more recently the industrial focus has moved to the methanol-to-olefins (MTO) process for the alternative production of light olefins. Light olefins, such as ethene and propene, are typically manufactured by hydrocarbon cracking and are key building blocks within the petrochemical industry.[1] Since methanol can be manufactured from natural gas,[2] coal or biomass,[3–5] the methanol-to-olefin process can be seen as an alternative to hydrocarbon cracking in a world where supplies of hydrocarbons derived from crude oil are dwindling.[1,6]

The MTO process involves catalysis over acidic zeolites. The selectivity to olefinic compounds is determined by zeolite topology and reaction operating conditions.[7] Traditionally, H-ZSM-5 has been the industrial catalyst of choice for MTO processes,[8–10] but more recently other zeolites, such as H-SAPO-34, have been widely investigated.[11–15] Zeolite H-ZSM-5 has an MFI-type structure with straight channels (0.51 nm × 0.54 nm) and intersecting sinusoidal channels. The pore architectures of H-ZSM-5 are well-defined, allowing shape selectivity in the MTO products.[16]

The mechanism of the MTO process has also been widely studied using a number of techniques,[17] such as isotopic labelling studies,[11–13,18] UV/Vis spectroscopy,[19–21] confocal fluorescence microscopy,[19,20] analysis of retained species,[12,13] NMR spectroscopy,[22] computational studies,[23] with the general conclusion that the MTO conversion relies on the so-called "hydrocarbon pool" (HCP) mechanism. The HCP mechanism involves the initial formation of dimethyl ether and water, followed by the formation of aromatic and higher olefin molecules from which alkenes are formed.[7,14,22,24–27] For MTO conversions using H-ZSM-5 catalysts, it has been shown that the formation of ethene from methanol progresses solely through an aromatic hydrocarbon pool mechanism which relies on poly-substituted methylbenzene molecules, while propene formation is linked to both the aromatic cycle and an olefin based cycle, as depicted in Figure 1.[7,15] Unlike other zeolite materials, the aromatic hydrocarbon pool mechanism over H-ZSM-5 has been shown to not include the highest substituted methylbenzene molecules (i.e., penta- and hexamethylbenzene), which are still formed within zeolite pores, but are virtually unreactive.[28]

With the increasing efforts towards the production of bio-ethanol—made from (hemi-)cellulose fermentation—as an al-

[a] Dr. E. Borodina, Dr. J. Ruiz-Martínez, Prof. Dr. B. M. Weckhuysen
Inorganic Chemistry and Catalysis Group
Debye Institute for Nanomaterials Science
Utrecht University, Sorbonnelaan 16, 3584 CA Utrecht (The Netherlands)
E-mail: b.m.weckhuysen@uu.nl

[b] Dr. E. C. Nordvang, Prof. Dr. R. Fehrmann
Centre for Catalysis and Sustainable Chemistry
DTU Chemistry, B. 207, Technical University of Denmark
2800 Kgs. Lyngby (Denmark)

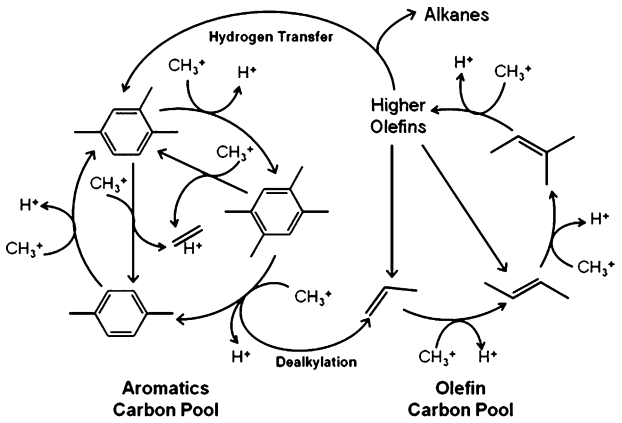

Figure 1. Dual olefin and aromatic methylation catalytic cycle for the methanol-to-hydrocarbons process on zeolite H-ZSM-5.[7]

ternative energy source, the ethanol-to-olefins (ETO) process has been gaining interest in recent years.[29–33] The ETO process, like the MTO process, requires an acidic catalyst such as an acidic zeolite.[34] The ETO process yields similar product distributions to the MTO process however, in the presence of ethanol, zeolite catalysts appear to deactivate much more rapidly, though this can be improved by the addition of water to the reaction feed.[35] The ETO process is thought to progress through a similar HCP reaction mechanism, with initial dehydration to ethene followed by formation of an aromatic hydrocarbon pool within the zeolite pores.[36–38] Deactivation of H-ZSM-5-based catalysts in ethanol also leads to increased selectivity towards ethene as the major product.[38,39] However, unlike the MTO process, the ETO process demonstrates irreversible deactivation at high reaction temperatures.[35]

Zeolites utilised in alcohol-to-hydrocarbons processes are increasingly deactivated with increasing time-on-stream and must be regenerated in order to regain their catalytic activity. In the case of H-ZSM-5, deactivation is thought to be caused by the formation of large poly-aromatic compounds (from the smaller aromatic molecules of the HCP mechanism) on the surface and in the pore openings of the catalyst in a process known as external coking.[26,28] Coking prevents the diffusion of reactants and products into and out of the zeolite channels, thus deactivating the catalyst.[7,15,19,20] Mores et al. found that the formation of coke on large zeolite H-ZSM-5 crystals could be probed using in situ UV/Vis spectroscopy and confocal fluorescence micro-spectroscopy.[19,20] The studies by Mores et al. showed that the intergrowth boundaries of large H-ZSM-5 crystals hinder the diffusion of aromatic species within the crystals. Additionally, the formation of graphite-like species on the surface and small aromatic inside the micropores were distinguished. Further investigations by Hofmann et al. applied the same large H-ZSM-5 crystals to a bulk MTO process in a fixed bed reactor and concluded that the bulk catalytic characteristics could be related to reactivity and coke formation in single-particle examinations.[40] Recently, Qian et al. published work comparing the formation of aromatic intermediate and coke species on large H-SAPO-34 crystals during MTO and ETO processes using a combination of UV/Vis micro-spectroscopy, confocal fluorescence microscopy and IR micro-spectroscopy.[18,41] The investigations by Qian et al. revealed that the formation of aromatic species during the MTO and ETO processes followed distinct reaction mechanisms, which lead to different coke formation profiles. Qian et al. concluded that the MTO process showed two distinct reaction phases: activation, when substituted methylated benzene carbocations were formed, and subsequent deactivation by the formation of poly-aromatic species at the outermost layers of the zeolite material. The ETO process, on the other hand consisted of only one stage, when methylated benzene carbocations and poly-aromatics were formed simultaneously, resulting in internal zeolite crystal coking.

The above-described studies of Mores et al. and Qian et al. show that micro-spectroscopy techniques are powerful characterization tools to understand the location, nature and mechanism of coke formation in zeolite crystals during alcohol-to-olefins reactions. However, previous studies have not (yet) established an intimate link between the spectroscopic information and catalytic performance. In this work, the next step is taken by combining operando UV/Vis spectroscopy with in situ UV/Vis and confocal fluorescence micro-spectroscopy. The approach taken is outlined in Figure 2. In this way, the catalytic performance of the zeolite material could be directly correlated with the spectroscopic characterization at a bulk level (i.e., a bed of large zeolite H-ZSM-5 crystals) and then compared with single H-ZSM-5 crystal micro-spectroscopy measurements.

As a result, a more consistent picture on the role of coke deposits on the catalytic performances and deactivation of large H-ZSM-5 crystals during alcohol-to-olefins reactions emerges.

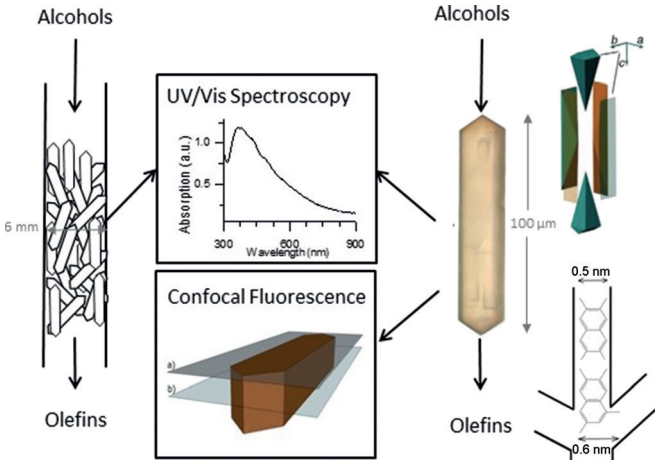

Figure 2. Schematic diagram of the experimental approach taken in this work. Left: operando UV/Vis measurements taken in a fixed bed reactor filled with a collection of single large zeolite H-ZSM-5 crystals during alcohol-to-olefins conversions (not to scale). Right: in situ UV/Vis and confocal fluorescence micro-spectroscopy measurements taken using single large zeolite H-ZSM-5 crystals during alcohol-to-olefins conversions. To the far right the crystal intergrowth structure of large H-ZSM-5 crystals can be seen (above) and a schematic diagram of formation of larger aromatic species in zeolite channel intercepts (below).

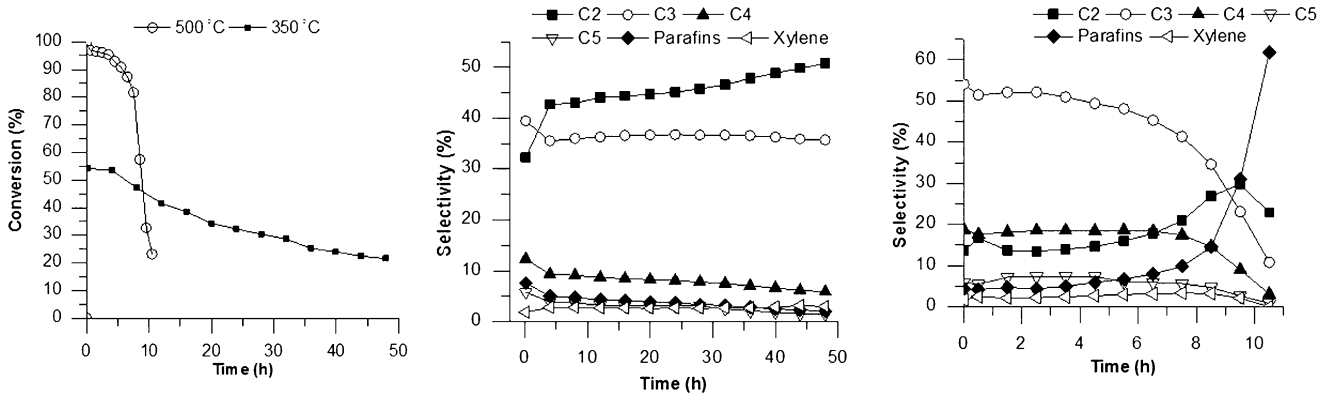

Figure 3. Conversion of methanol (left) and selectivity of the methanol-to-olefins (MTO) conversion over a collection of single large zeolite H-ZSM-5 crystals to C2-5 compounds, paraffins and xylene during MTO catalytic test on fixed bed reactor at 350 °C (middle) and 500 °C (right).

Results

Operando UV/Vis spectroscopy measurements

The catalytic performance of large H-ZSM-5 crystals for MTO and ETO conversions at 350 and 500 °C are shown in Figure 3 and Figure 4, respectively. The operando UV/Vis spectra taken during the MTO and ETO catalytic tests are summarized in Figure 5.

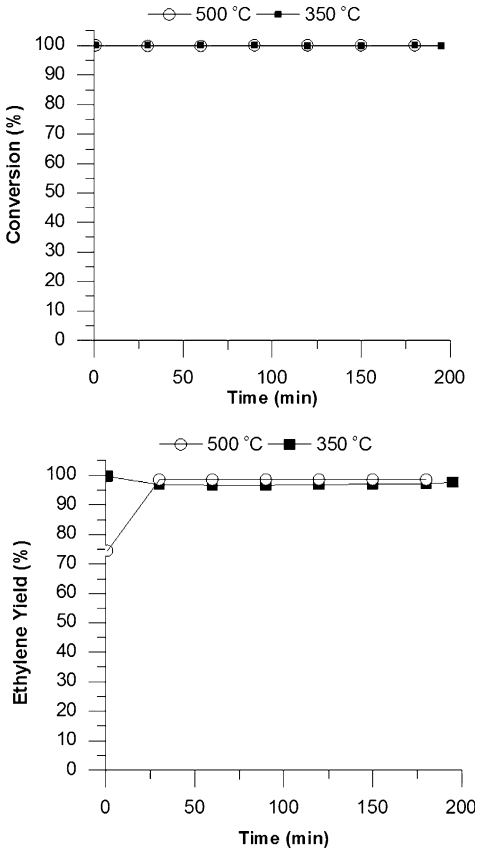

Figure 4. Conversion of ethanol (top) and selectivity to ethene (bottom) during the ethanol-to-olefins (ETO) catalytic testing over a collection of single large zeolite H-ZSM-5 crystals in a fixed bed reactor at 350 and 500 °C.

In order to better analyse the obtained UV/Vis spectra, they were deconvoluted in a similar manner to previously reported data,[18,19] using Gaussian functions determined by the shape of the UV/Vis absorption spectra. The positions and widths of the Gaussian bands used are described in Table 1.

An additional, extremely broad band was used as a baseline in all cases. The results of the deconvolution of the operando UV/Vis spectra are shown in Figure 6. The individual Gaussian bands contributing to the UV/Vis spectra have previously been attributed to π–π^* transitions of specific carbonaceous species present on the surface and in the pores of the crystal.[19,20,23,25,26,42] The UV/Vis band at around 400 nm, has been assigned to π–π^* transitions of methyl-substituted benzene cations. Some methyl-substituted benzenes are thought to constitute a catalytic scaffold in the HCP mechanism over H-ZSM-5.[23,25,26,28,42] Bands at higher wavelengths (450, 510 and 595 nm) can be assigned to larger aromatic species including naphthalenes and anthracenes,[23,26,42] while baseline contributions can be assigned to more extended poly-aromatic and/or graphite-like species.

In agreement with previous studies,[40] Figure 3 shows that methanol is converted to various olefins over large H-ZSM-5 crystals at 350 and 500 °C. As was previously observed, at 350 °C the initial conversion was moderate (54%) and deactivation was slow, giving 20% conversion after 50 h on stream, whereas at 500 °C the conversion was initially very high (97%) but declined rapidly after 8 h on stream. As shown by the UV/Vis spectra in Figure 5 and the deconvolution data in Figure 6, the formation of large aromatic and graphite-like coke species with increasing time-on-stream is observed. During the MTO conversion at 350 °C there is a gradual intensity increase in the UV/Vis bands representing large aromatic species (510, 595 nm and baseline contributions), whereas at 500 °C there is rapid development of the UV/Vis bands representing poly-aromatic/graphite-like species (baseline contributions), indicating rapid coking and deactivation.

During MTO conversions at both 350 and 500 °C there was a high selectivity to light olefins. The C2 and C3 products detected were almost exclusively ethene and propene, respectively. The constant high selectivity to light olefins at 350 °C

Table 1. Overview of the positions of Gaussian functions used for the deconvolution of the UV/Vis absorption spectra of large H-ZSM-5 crystals during MTO and ETO processes at 350 and 500 °C.[a]

Conversion process	Gaussian bands [nm]	
	350 °C	500 °C
MTO (operando catalytic tests)	410 (39), 450 (46), 510 (55), 595 (60)	418 (39), 450 (46), 510 (55), 595 (60), 650 (62)
ETO (operando catalytic tests)	418 (26), 450 (46), 510 (50), 552 (38), 599 (32), 650 (37)	418 (26), 450 (46), 510 (50), 552 (38), 599 (32), 650 (37)
MTO (in situ micro-spectroscopy)	403–410 (39), 450 (46), 510 (55), 595 (60)	416–422 (24), 450 (46), 510–513 (55), 587–595 (60), 650 (62)
ETO (in situ micro-spectroscopy)	407–417 (26), 449–452 (44), 510–518 (50), 552–553 (38), 597–599 (32), 651–656 (37)	403–418 (28), 457–463 (44), 509–510 (48), 552 (38), 602–603 (35), 656 (38)

[a] Numbers in parentheses indicate the band widths of the Gaussian functions.

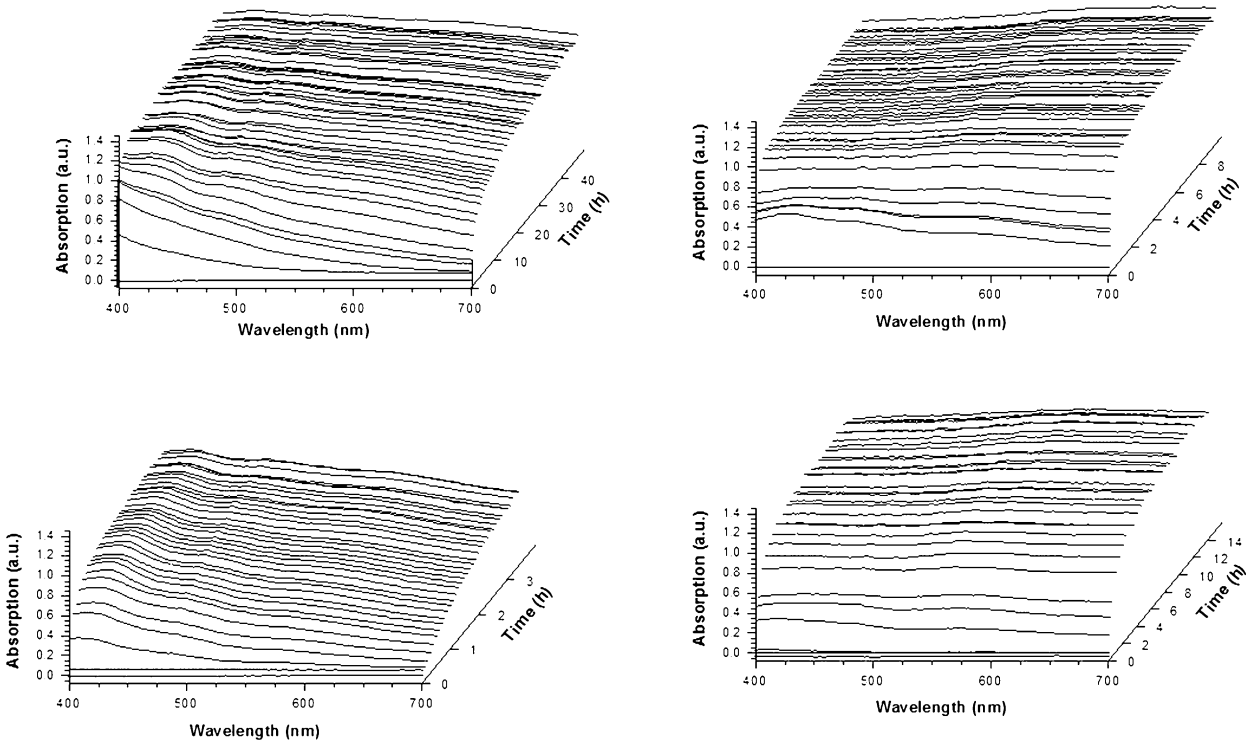

Figure 5. UV/Vis absorption spectra taken during the methanol-to-olefins (MTO; top two figures) and ethanol-to-olefins (ETO; bottom two figures) catalytic testing over a collection of single large zeolite H-ZSM-5 crystals loaded in a fixed bed reactor at 350 °C (left two figures) and 500 °C (right two figures).

did not change with increasing time-on-stream, which is agreement with the relatively stable conversion of methanol and the absence of deactivation. During the MTO conversion at a reaction temperature of 500 °C, there was initially very high selectivity to propene, which decreased rapidly, whilst selectivity to ethene increased slightly and selectivity to paraffins (mainly methane) increased significantly in the later stages of the process.

As shown in Figure 4, conversion of ethanol during ETO reactions in a fixed-bed reactor was constant at >99% for both reaction temperatures (350 and 500 °C). Ethene selectivity was also constant at >96% after 1 h on stream, indicating that ethene is the dominant product formed. Small contributions to the product distributions came from propane, propene, butane, paraffins and xylene. In contrast to the MTO reaction, there was little variation in selectivity, stability or activity shown when the temperature was changed from 350 to 500 °C. However, there was one small difference between the catalytic results of the ETO conversion at 350 and 500 °C: as can be seen in Figure 4, the initial selectivity towards ethene was slightly lower at 500 °C (74%) than 350 °C (100%) at 1 h on stream. The reduced selectivity to ethene at 1 h on stream at 500 °C was mostly due to the formation of methane (20%).

Despite little variation in the catalytic results of the ETO conversion at 350 and 500 °C, there were obvious differences observed in the operando UV/Vis spectra measured at each temperature. At 350 °C, the UV/Vis spectra showed the formation of an absorption band at a lower wavelength (410–420 nm),

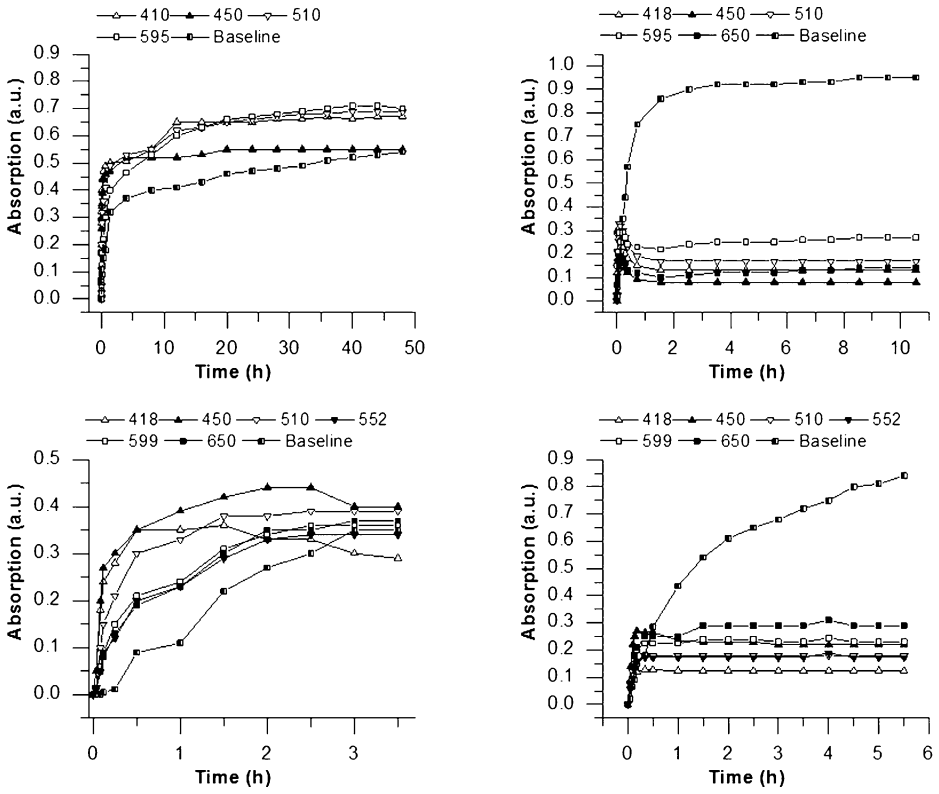

Figure 6. Time development of the normalized Gaussian functions from the deconvoluted UV/Vis spectra obtained during catalytic testing of a collection of single large zeolite H-ZSM-5 crystals loaded in a fixed bed reactor during the MTO conversion at 350 °C (left top) and 500 °C (right top) and ETO conversion at 350 °C (left below) and 500 °C (right below).

with a shoulder at 510–520 nm, followed by the growth of contributions at higher wavelengths (i.e., 550 and 620 nm) and baseline contributions. However, at 500 °C, the UV/Vis spectra taken during the ETO conversion were rapidly dominated by baseline contributions. Although a broad low wavelength band at around 415 nm was observed at first, by 1 h on stream, no absorption bands were observed, only an increased baseline.

Single crystal in situ UV/Vis and confocal fluorescence microscopy

The microphotographs and UV/Vis spectra obtained during the MTO conversion at 350 and 500 °C (Figure 7) were in agreement with those previously reported in literature by Mores et al. and those seen during the bulk catalytic testing experiments.[19,20] The in situ UV/Vis spectra were also deconvoluted with the same band positions and widths as in the operando UV/Vis measurements described above (Table 1). The results of the deconvolution of the in situ UV/Vis spectra are plotted in Figure 6.

During the MTO conversion at 350 °C, the zeolite H-ZSM-5 crystals appeared increasingly orange/brown with increasing time-on-stream under reaction conditions, the increase in orange colour in the microphotographs was accompanied by the appearance and gradual growth of a major absorption band at approximately 405 nm in the UV/Vis spectra. Furthermore, slow development of less defined absorption bands at higher wavelengths and a slight increase in the baseline level of absorbance was observed with increasing time-on-stream under reaction conditions. Such observations can also be seen from the deconvolution UV/Vis band intensities with increasing time-on-stream (Figure 6). While early UV/Vis spectra were dominated by the low wavelength band at 403–410 nm, higher wavelength bands and baseline contributions increased with time-on-stream during the MTO conversion at 350 °C. However, the increasing intensity of higher wavelength bands did not appear to be at the expense of the low wavelength 403–410 nm band, which continued to increase in intensity throughout the tested time under reaction conditions. The increase in the overall absorption of UV/Vis light during the MTO conversion at 350 °C, shown in UV/Vis spectra and deconvolutions as baseline contributions and present in microphotographs as a grey colour, suggests the presence of condensed aromatic rings in graphite-like structures.[19,25]

The microphotographs and UV/Vis spectra taken during the MTO process at 500 °C contrasted with those at 350 °C. Both the microphotographs and UV/Vis spectra showed much more rapid crystal darkening at 500 °C. Although a low wavelength absorption band (416–422 nm) and higher wavelength absorption bands (450, 587–595, 650 nm) were evident initially, the UV/Vis spectra quickly became dominated by baseline contributions, with reduced intensities of the other absorption bands. The defined absorption bands that contribute to the UV/Vis spectra in the first few minutes under reaction conditions decreased in intensity after less than 10 min on stream. The apparent reduction in intensity of absorption bands contributing to the UV/Vis spectra was most likely due to the formation of poly-aromatic coke species on the surface of the zeolite H-ZSM-5 crystal blocking the absorption of light by smaller aromatic species within the crystal. By comparison to UV/Vis observations of the MTO conversion at 350 °C, the UV/Vis spectra of the MTO conversion at 500 °C showed an additional band at 650 nm. The formation of an additional absorption band at a higher wavenumber may indicate the formation of a larger aromatic compound, for example species with four fused benzene rings.[19,20,23] Baseline contributions to the UV/Vis spectra during the 500 °C MTO conversion process increased rapidly

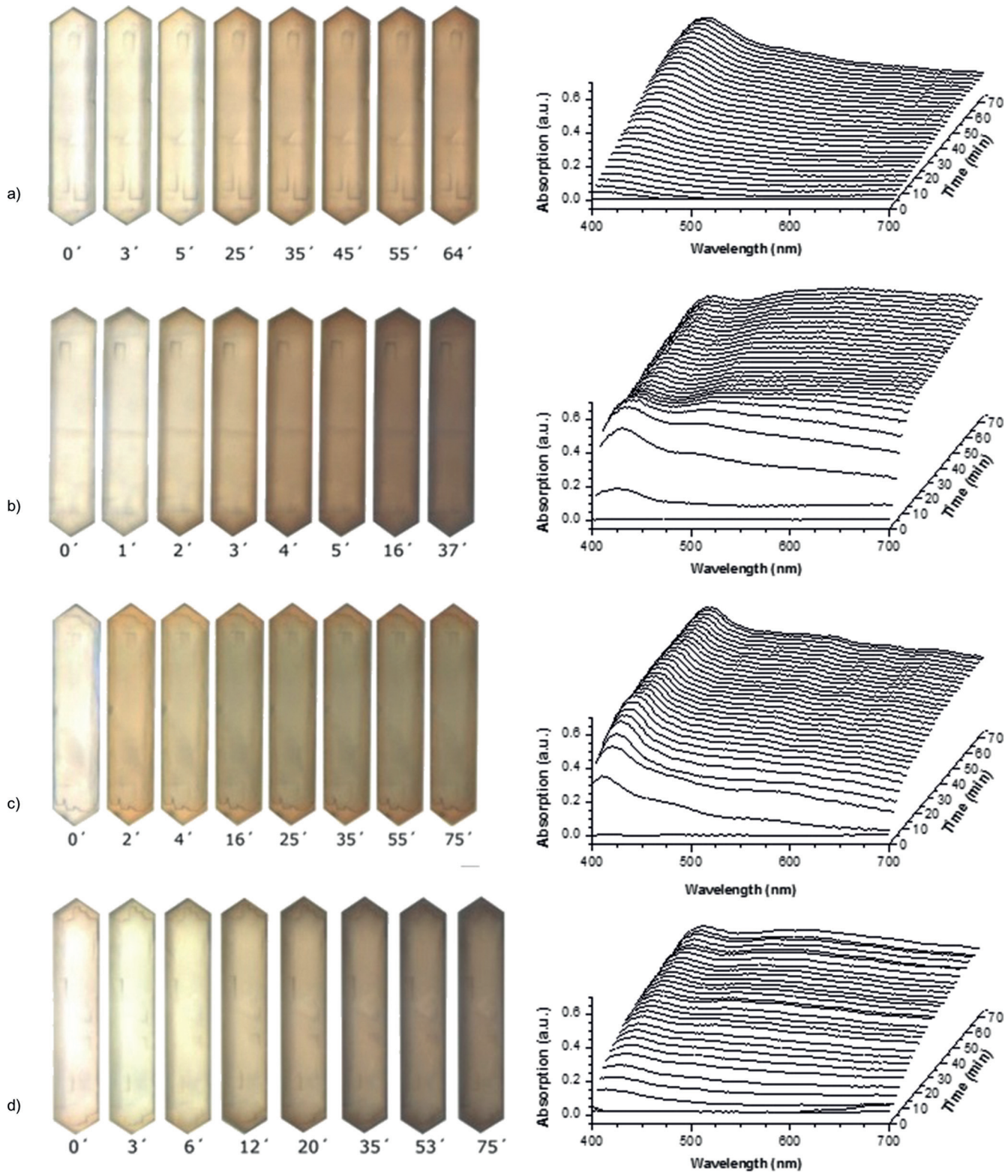

Figure 7. Optical microphotographs (left) and UV/Vis absorption spectra (right) taken in situ during the MTO conversion at: a) 350 °C, and b) 500 °C, and ETO conversion at: c) 350 °C, and d) 500 °C over single large zeolite H-ZSM-5 crystals. The corresponding time is indicated in minutes.

over the first 20 min under reaction conditions and then remained high for the rest of the tested reaction time. The presence of a high baseline absorbance, which is translated into the greyer colour of the crystals seen in the microphotographs, suggests the extensive presence of large poly-aromatic species.

At 350 °C under ETO conversion conditions, the zeolite H-ZSM-5 crystals became discoloured very quickly, with an obvi-

ous orange/brown colour after only 2 min under reaction conditions, as shown by Figure 7c. As with the spectra taken during the MTO conversion, the UV/Vis spectra taken during the ETO conversion at 350 °C were dominated by the presence of a low wavelength band at 407–417 nm, suggesting the presence of protonated poly-alkylated benzenes.[26] Other, higher wavelength bands (449–452, 510–518, 552–553, 597–599, 651–656 nm) also developed during the first 10 min of reaction time and then remained relatively constant for the rest of the time under reaction conditions. The baseline contributions also developed quickly within the first 10 min of reaction time, but continued to increase in intensity more gradually. By comparison to UV/Vis observations of the MTO conversions at reaction temperatures of 350 and 500 °C, the UV/Vis spectra of the ETO conversion at 350 °C showed an additional absorption band at 552–553 nm, while the absorption band observed at approximately 595 nm during MTO conversions was shifted to about 599 nm during ETO conversion at 350 °C. The additional bands seen in the UV/Vis spectra during ETO in comparison to MTO could be due to variations in the aromatic species formed inside the zeolite, including the presence of ethyl-substituted aromatics. Such ethyl-substituted aromatics have been observed previously but are not thought to participate in the ETO reaction mechanism, though they may function as coke precursors.[38] At 350 °C, baseline contributions to the UV/Vis spectra appeared to develop much more rapidly during the ETO conversion than during the MTO conversion, suggesting more rapid external coke formation. More rapid coke formation during ETO by comparison to MTO is in line with literature observations that H-ZSM-5 catalysts deactivate much more quickly during ETO than MTO (Figures 7 and 8).[38]

In agreement with the operando UV/Vis spectra taken during catalytic testing, the in situ UV/Vis spectra measured during ETO at 500 °C were dominated by baseline contributions, making it difficult to identify any distinct contributing absorption bands and indicating a high level of external coking. While the baseline contributions increased throughout the reaction time, the other contributing absorption bands appeared to reach maximum intensity by 15–20 min under reaction conditions and then maintain relatively constant intensities.

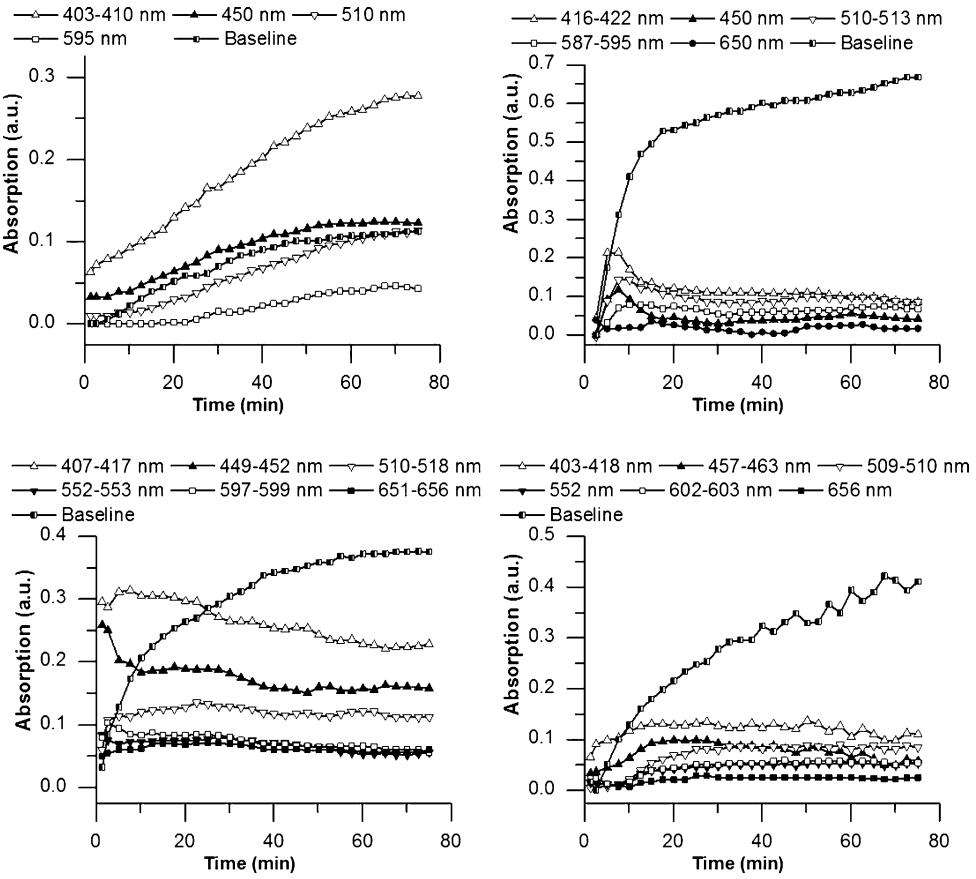

Figure 8. Time development of the normalized Gaussian functions from deconvoluted UV/Vis spectra taken in situ during the MTO conversion at 350 °C (left top) 500 °C (right top) and ETO conversion at 350 °C (left below) 500 °C (right below) over single large H-ZSM-5 crystals.

In situ single crystal confocal fluorescence micro-spectroscopy

Zeolite H-ZSM-5 crystals were exposed to methanol or ethanol and studied under reaction conditions with confocal fluorescence microscopy. The samples were irradiated with laser light sources at 405, 488 and 561 nm and the fluorescent light emitted was detected within the ranges 425–475, 510–550 and 575–635 nm, respectively. None of the exciting laser wavelengths showed significant fluorescence before introduction of methanol or ethanol to the in situ cell and the small amount of fluorescence that was observed prior to methanol/ethanol addition can be assigned to small amounts of remaining template material or related organic impurities from the zeolite synthesis process.

During the MTO conversion at a reaction temperature of 350 °C, vast differences were noted for the different zeolite crystal planes, laser energies and reaction times. Fluorescence intensities at the centre of the crystal planes can be seen in Figure 11, while the distribution of fluorescence across the crystal planes are plotted in Figure 9. Within 2 min under MTO reaction conditions, an increase in fluorescence was obvious for both zeolite crystal planes. The fluorescence of the zeolite crystals after exposure to methanol has been previously assigned to the presence of large coke species and their precursors, with increasing excitation wavelengths exciting more-ex-

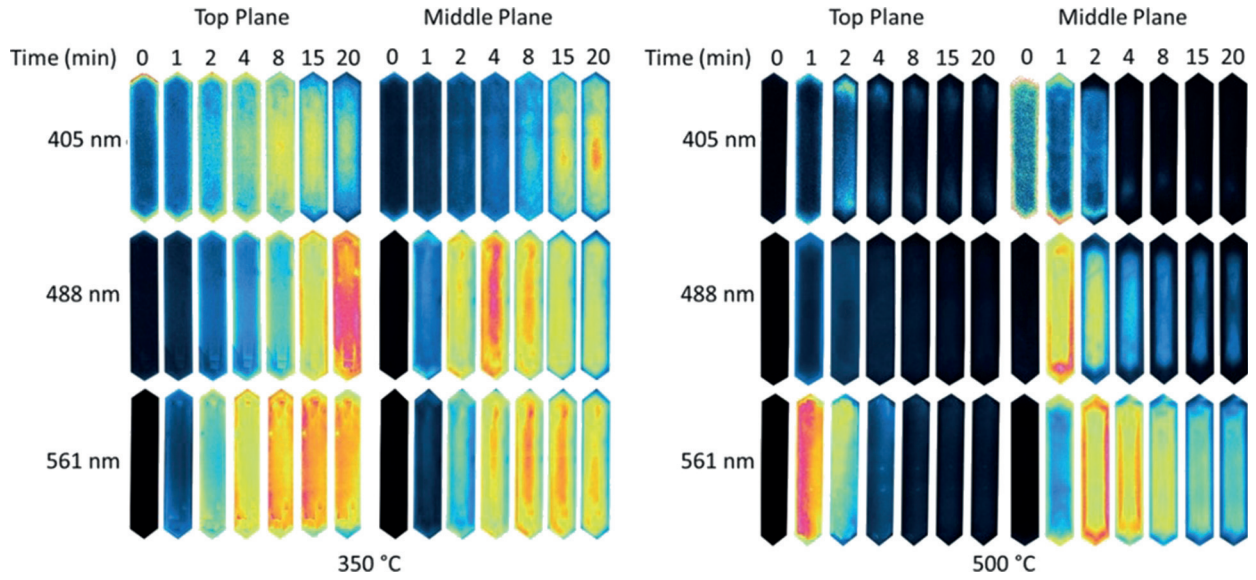

Figure 9. Distribution of fluorescence intensity from single large zeolite H-ZSM-5 crystals irradiated with laser light sources at 405, 488 and 561 nm and emissions were detected within the ranges 425–475, 510–550 and 575–635 nm, respectively, in different crystal planes and at varying reaction times during MTO at 350 and 500 °C. Images have been adjusted to show change in distribution and intensity of fluoresce for each laser energy and crystal plane and therefore intensities are not comparable for different planes and/or lasers.

tended coke compounds.[20,43] There was a general increase in overall fluorescence with increasing time-on-stream, which is in agreement with the observations made from the corresponding UV/Vis spectra.

A 405 nm laser is thought to excite small aromatic species formed as part of the HCP mechanism and as precursors to larger aromatic coke species.[20] During MTO at 350 °C, the 405 nm laser yielded the lowest fluorescence intensity on both the surface and middle crystal planes, which may be due to poor laser efficiency or a low quantum yield for the fluorescent species. For both crystal planes, fluorescence resulting from exposure to the 405 nm laser appeared first at the edges of the zeolite crystal. After 15 min under reaction conditions the fluorescence become visible in the centre of the zeolite crystal and expand towards the crystal edges. For excitation of the H-ZSM-5 crystals with the 488 nm laser during the MTO conversion at a reaction temperature of 350 °C, there was a marked difference in fluorescence intensity and distribution between the middle and top planes of the zeolite crystal. The fluorescence intensity resulting from excitation with the 488 nm laser was much more intense from the middle plane of the crystal than the top plane. Furthermore, in the middle plane the fluorescence intensity was concentrated in the centre of the zeolite crystal, along the intersection of the inter-growing crystals, while on the surface plane of the crystal the fluorescence was more evenly spread across the whole crystal plane. Previous studies suggested that the 488 nm laser excites larger charged aromatic molecules with two fused benzene rings and varying degrees of methylation.[20,23] The distribution of species excited by the 488 nm laser suggests that some of the species may be too large to exist in the straight, 0.51 nm × 0.54 nm H-ZSM-5 channels and may only exist at channel intercepts or defects. This may be case for aromatic molecules with two fused benzene rings and methyl groups in positions hindering their ability to fit in the straight channels, as shown in Figure 2. This observation is in agreement with the previous work of Brogaard et al., who concluded from computational studies that the preferred absorption sites of aromatics in H-ZSM-5 is at the intersection of straight and sinusoidal channels.[44]

Upon observation of the fluorescence intensities during MTO conversion at a reaction temperature of 350 °C, the most obvious observation was the significantly higher fluorescence resulting from excitation with the 561 nm laser in comparison to the other lasers used, this may be due to high laser efficiency or high quantum yield of the excited species. The distribution of fluorescence on the two planes was similar to that observed when excited with the 488 nm laser, with the fluorescence concentrated in the centre of the middle plane and spread more evenly on the surface plane. It has been suggested that the 561 nm laser excites larger cationic aromatic molecules with two fused benzene rings with a methylation degree of five or higher or three fused benzene rings with various degrees of methylation.[20,23] It is also possible that the fluorescence seen in the centre of the zeolite H-ZSM-5 crystal is due to the presence of aromatic species in larger cavities at the intergrowth crystal boundaries within the large H-ZSM-5 crystal.

At a reaction temperature of 500 °C the confocal fluorescence microscopy observations were quite different to those seen at 350 °C, as shown by Figure 9 and Figure 11. The fluorescence light was observed at much shorter reaction times and faded on the top plane after 2 min on stream, suggesting the formation of more extended non-fluorescent species, for example, graphite-like species. In agreement with the higher reaction temperature applied, the kinetics of the formation fluorescent species was faster at 500 °C than at 350 °C. For all lasers, the observations differed from those obtained at low re-

action temperature with respect to coke distribution. The fluorescence in the middle plane appeared first in a shell around the edges of the zeolite crystal and moved towards the centre of the crystal. With increasing time-on-stream, the fluorescence at the exterior crystal shell decreased due to the formation of more extended poly-aromatic species. Then, the fluorescence in the middle of the zeolite H-ZSM-5 crystal also gradually faded, which may be due to the conversion of the aromatic species into more bulky, non-fluorescent aromatics and/or the large poly-aromatics on the shell of the crystal reabsorbing the fluorescent light and therefore decreasing the light reaching the fluorescence detector. In contrast to previous observations, at 500 °C during the ETO conversion, fluorescence formed strongly around the edge of the zeolite crystal and then migrated towards the centre for all exciting laser wavelengths and both crystal planes, as shown in Figure 10. The fluorescence intensity generally seemed to peak in intensity at approximately 1–2 min, followed by a general decrease, though this was not reflected in the intensity measurements from the centre of each plane as shown in Figure 11. Interestingly, the fluorescence originating from the 488 nm laser seemed to peak in intensity indicating the formation of larger aromatic compounds with increasing time-on-stream. The reduction in intensity after 2 min on stream may be due to the formation of graphite-like structures, which are non-fluorescent or due to the cracking of larger aromatics into smaller non-fluorescent organics.

Discussion

The studies presented confirm that large H-ZSM-5 crystals are catalytically active in both MTO and ETO processes at reaction temperatures of 350 and 500 °C and therefore are suitable model systems for use in single crystal spectroscopic investigations, such as those conduced previously by Mores et al.[19,20] and Hofmann et al.[40] It is clear from the combined catalytic testing results and operando UV/Vis results that the formation of coke species during the MTO conversion over large H-ZSM-5 crystals can be correlated with catalyst deactivation. This conclusion substantiates the previous work by Hofmann et al., where catalytic testing results and UV/Vis spectroscopy results were linked but not conduced simultaneously.[40] The present results display the similarities between UV/Vis spectra collected during catalytic tests as operando measurements and those collected during single crystal in situ measurements that allow spatiotemporal observations.

The increasing presence of larger aromatic species and graphite-like species with increasing time-on-stream under reaction conditions observed by operando UV/Vis spectroscopy, single crystal in situ UV/Vis micro-spectroscopy and confocal fluorescence microscopy suggests large aromatic species are built from smaller species already present on the surface and/or in the pores of the zeolite catalyst. Since such large aromatics and graphite-like structures are too large to be formed inside the zeolite H-ZSM-5 crystal, they must be formed on the outer surface of the zeolite catalyst and therefore contribute to pore blocking and catalyst deactivation. For both the MTO and ETO conversions, it as noted that coke formation happened more rapidly at 500 °C than at 350 °C.

In contrast to the work by Qian et al., who observed that large aromatic and coke species on large H-SAPO-34 crystals during MTO developed mainly on the shell of the crystal, we observed that at 350 °C aromatic species appear to be first produced at the centre of the large H-ZSM-5 crystals and then dif-

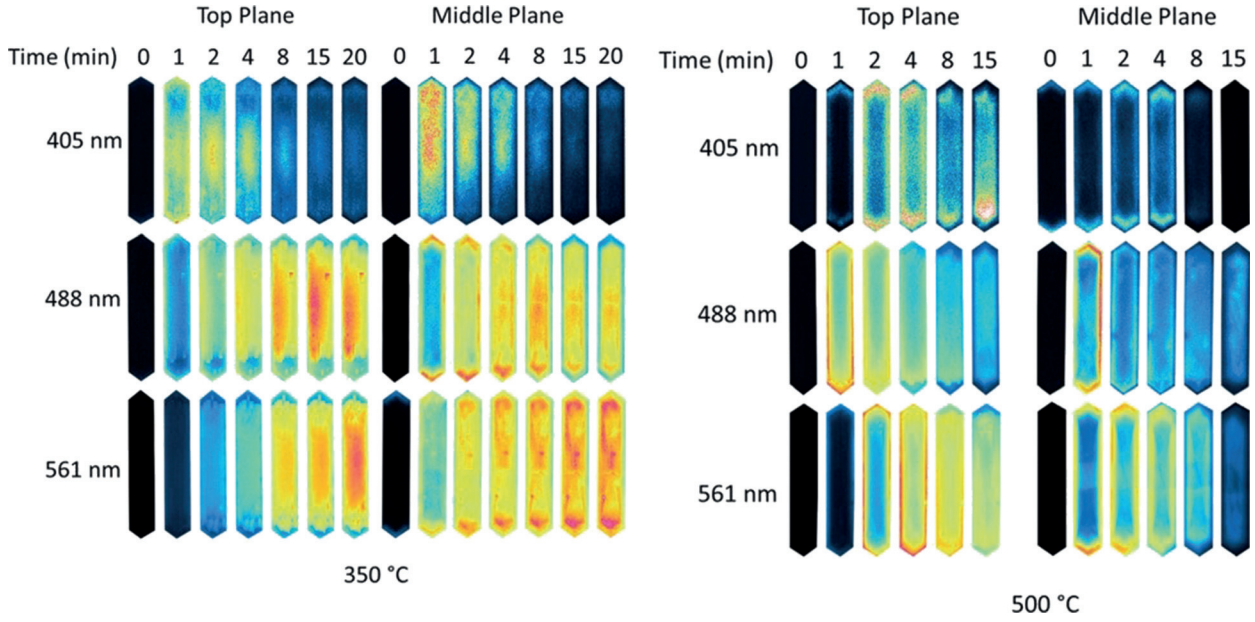

Figure 10. Distribution of fluorescence intensity from single large zeolite H-ZSM-5 crystals irradiated with laser light sources at 405, 488 and 561 nm and emissions were detected within the ranges 425–475, 510–550 and 575–635 nm, respectively, in different crystal planes and at varying reaction times during ETO at 350 and 500 °C. Images have been adjusted to show change in distribution and intensity of fluoresce for each laser energy and crystal plane and therefore intensities are not comparable for different planes and/or lasers.

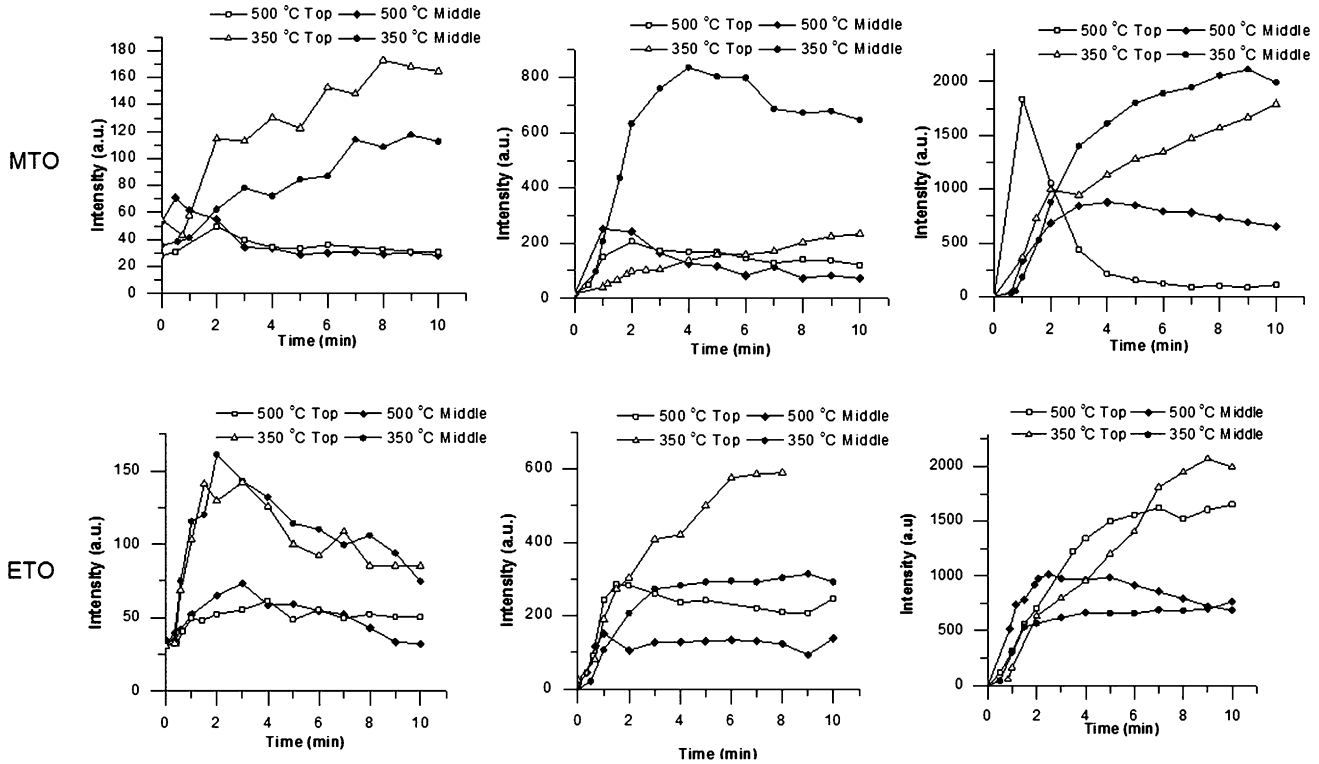

Figure 11. Time development of fluorescence intensity from lasers at 405 (left), 488 (middle) and 561 nm (right) in their corresponding detection zones. The measurements were taken in the middle of the zeolite H-ZSM-5 crystal on both the surface (top) plane of the crystal and in the middle plane of the zeolite H-ZSM-5 crystal for MTO (above) ETO (below) conversions at 350 and 500 °C.

fuse towards the crystal shell. The differences in the diffusion properties and micropore sizes of both type of crystals may account for the changes in the distribution of aromatic species. In this way, the large cavities and small windows of H-SAPO-34 allow the formation and growth of aromatic species in the outer layers of the material but not their molecular transport inwards, which is going to block the micropore structure of the material. Conversely, the H-ZSM-5 micropore network allows the diffusion of mono-aromatic species throughout the crystal and hinders the growth of those into more extended and deactivating species. This explains the difference in aromatic distribution and catalyst lifetime in both framework topologies; that is, CHA versus MFI.

UV/Vis and confocal fluorescence microscopy of the MTO conversion at 500 °C indicate that under these conditions methanol is rapidly converted into aromatic species around the edges. Then, the aromatics diffuse out of the zeolite and react forming large poly-aromatic coke species on the zeolite external surface, blocking the crystal pores and hence limiting diffusion of reactants and products into and out of the crystal. Aromatic coke species on the outer edges of the crystals are not constrained in size by the zeolite pores and therefore quickly became larger.

The product distributions of the MTO conversions observed during catalytic testing along with operando UV/Vis measurements provide details about the reaction mechanism. A dual cycle concept is proposed to be the dominant mechanism for production of light olefins over large H-ZSM-5 crystals,[28] where the "methylated benzenes cycle" leads to the production of ethene and the "higher alkenes cycle" contributes to the production of propene. During MTO at 350 °C, there is a high selectivity to ethene, suggesting the dominance of the "methylated benzenes cycle". The significant presence of methylated benzene molecules during reaction conditions at 350 °C, as observed by UV/Vis spectroscopy (both operando and single crystal in situ) and confocal fluorescence microscopy, supports the major contribution of the "methylated benzenes cycle". At a reaction temperature of 500 °C, the high selectivity to propene indicates that the main catalyst mechanism is the "higher alkene" cycle, this is further substantiated by UV/Vis and confocal fluorescence microscopy observations where absorption bands corresponding to methylated benzene carbocations remain low under reaction conditions.

The catalytic testing and spectroscopic results of the ETO conversion are quite different to those observed during the MTO conversion. The high selectivity to ethene is observed at both 350 and 500 °C with rapid formation of graphite-like coke species. The high selectivity to ethene combined with the significant presence of coke species suggests that ethene is formed simply by dehydration and perhaps to some extent by cracking of larger aromatic species. Cracking and formation of ethene does not appear to be the predominant mechanism during MTO at 500 °C, therefore if cracking occurs during ETO at 500 °C it may be due to the differences in the nature of the present aromatic species.

Conclusion

In this work, the catalytic activity of large H-ZSM-5 crystals in MTO and ETO conversions has been tested. Using operando UV/Vis measurements, we have successfully correlated the formation of coke (precursors) on the zeolite external surfaces during progressive zeolite deactivation. Furthermore, this approach allowed the proposal of a dual cycle mechanism with an olefin carbon pool favouring propene production and methylated benzenes carbon pool, enhancing the formation of ethane to be substantiated. We can also confirm that coke (precursor) species are formed from smaller aromatic species in the aromatic carbon pool.

We have investigated, in a spatiotemporal manner, the intermediates and coke formation in situ in individual zeolite H-ZSM-5 crystals with UV/Vis and confocal fluorescence microspectroscopy. It was observed that rapid deactivation at a reaction temperature of 500 °C was due to the fast formation of aromatic species in the outermost layers of the zeolite H-ZSM-5 crystal and subsequent formation of poly-aromatic species on the external surface, preventing diffusion of reactants and products into and out of the crystal.

Finally, operando UV/Vis spectroscopy results observed during catalytic testing have been correlated with single crystal in situ results, confirming that the use of large H-ZSM-5 crystals as model crystals in in situ spectroscopic studies can be related to results obtained in a fixed bed reactor set-up.

Experimental Section

Materials

Large zeolite ZSM-5 crystals (Si/Al ratio of **17**, 100 μm × 20 μm × 20 μm) were provided by ExxonMobil (Machelen, Belgium). The starting materials for the synthesis of the ZSM-5 crystals were: Ludox AS-40, tetrapropylammonium (TPA) bromide (TPABr, Fluka), $Al_2(SO_4)_3 \cdot 18\,H_2O$ (Baker), and NH_4OH (29%). The molar composition was $6.65\,(NH_4)_2O/0.67\,TPA_2O/0.025\,Al_2O_3/10\,SiO_2/121\,H_2O$. For synthesis, Ludox AS-40 and TPABr were mixed. Subsequently, $Al_2(SO_4)_3 \cdot 18\,H_2O$ was added and mixed for 5 min, followed by the addition of NH_4OH and further mixing for 7 min. Heating was carried out starting from room temperature up to 178 °C, which took 2 h (7 days soak time under static conditions), followed by washing and drying at 120 °C for 12 h. The as-prepared ZSM-5 zeolite crystals were calcined, first by preheating them at 120 °C (30 min, 2 °C min^{-1}) and then by increasing the temperature to 550 °C (360 min, 10 °C min^{-1}). This was followed by a triple ion exchange with a 10 wt.% ammonium nitrate (Acros Organic, 99+%) solution at 80 °C. Subsequently, a second calcination was performed to obtain the ZSM-5-P sample. Methanol was obtained from Sigma–Aldrich, HPLC grade 99.8%. Ethanol was obtained from Interchema, 100%. Both ethanol and methanol were used as received.

Fixed bed reactor testing with on-line operando UV/Vis spectroscopy

Catalytic activity measurements were carried out in a quartz fixed-bed reactor. Large zeolite ZSM-5 crystals (25 mg) were loaded and activated at 550 °C under oxygen for 1 h and then cooled until the reaction temperature of 350 and 500 °C. A $WHSV_{Alcohol}$ of 6 g g^{-1} h^{-1} was obtained by flowing He gas through a saturator filled with methanol or ethanol at 20 °C. Analysis of the reactant and products was performed with gas chromatography (GC; Interscience, Compact GC) equipped with Rtx-1 + Rtx-Wax columns and Rt-TCEP + Rtx-1, and Al_2O_3/Na_2SO_4 columns, respectively, and two FID detectors. Methanol/ethanol conversion was determined by analysis of the reactor feed before and during the reaction and dimethyl ether was considered as a reactant due to its role in the reaction mechanism. Operando UV/Vis spectra were taken every 30 s at the beginning of the MTO/ETO reaction then the time interval was increased up to 300 s, with 70 accumulations of 50 ms exposure time each.

Single zeolite H-ZSM-5 crystal optical micro-spectroscopy

The UV/Vis micro-spectroscopy measurements were performed with an Olympus BX41 upright microscope using a 50×0.5 NA high working-distance microscope objective lens. A 75 W tungsten lamp was used for illumination. In addition, the microscope has a 50/50 double viewpoint tube, which accommodates a CCD video camera (ColorView IIIu, Soft Imaging System GmbH) and an optical fibre mount. A 200 μm core fibre connects the microscope to a CCD UV/Vis spectrometer (AvaSpec-2048TEC, Avantes BV). The large zeolite H-ZSM-5 crystals were loaded into an in situ cell (Linkam FTIR 600) equipped with a temperature controller (Linkam TMS 93). The crystals were placed in a flow of 10 mL min^{-1} O_2/40 mL min^{-1} N_2 and heated to 500 °C at a rate of 15 min^{-1}, the crystals were kept at this temperature for 1 h before cooling to required reaction temperature (at a rate of 15 min^{-1}). Once the reaction temperature was achieved, the flow was changed to 50 mL min^{-1} N_2 only. Subsequently, the N_2 flow was diverted through a bubbler containing methanol or ethanol for the desired reaction time.

Single zeolite H-ZSM-5 crystal confocal fluorescence microscopy

Confocal fluorescence microscopy studies were performed with a Nikon Eclipse LV150 upright microscope with a 50×0.55 NA dry objective lens. The confocal fluorescence images were collected with the use of a Nikon-Eclipse C1 head connected to the laser light sources (405, 488 and 561 nm). The emission was detected with three photomultiplier tubes in the range 425–475, 510–550 and 575–635 nm for the three lasers, respectively (in order to avoid channel overlap). Large zeolite ZSM-5 crystals were loaded into an in situ cell (Linkam FTIR 600) equipped with a temperature controller (Linkam TMS 93). The crystals were placed in a flow of 50 mL min^{-1} O_2 and heated to 500 °C at a rate of 15 °C min^{-1}, the crystals were kept at this temperature for 1 h before being cooled to required reaction temperature (at a rate of 15 °C min^{-1}). Once the reaction temperature was achieved, the flow was changed to 50 mL min^{-1} N_2 only. Subsequently, the N_2 flow was diverted through a bubbler containing methanol or ethanol for the desired reaction time. The fluorescence intensity was measured across both the middle and surface (top) planes of the zeolite H-ZSM-5 crystals (Figure 2) at varying times under reaction conditions.

Acknowledgements

This work was supported by The Netherlands Research School Combination-Catalysis (NRSC-C) and a European Research Council (ERC) Advanced Grant (no. 321140). E.C.N. thanks the

European Community for funding from the Seventh Framework Programme [FP7/2007-2013] for SYNFLOW under grant agreement no. NMP2-LA-2010-246461. J.R.-M. thanks CW-NWO for a VENI grant. The authors acknowledge Machteld Mertens (ExxonMobil, Machelen) for providing the large zeolite H-ZSM-5 crystals.

Keywords: methanol-to-olefins · fluorescence microscopy · heterogeneous catalysis · UV/Vis spectroscopy · zeolites

[1] R. Diercks, J.-D. Arndt, S. Freyer, R. Geier, O. Machhammer, J. Schwartze, M. Volland, *Chem. Eng. Technol.* **2008**, *31*, 631 – 637.
[2] D. A. Hickman, L. D. Schmidt, *Science* **1993**, *259*, 343 – 346.
[3] D. Güllü, A. Demirbaş, *Energy Convers. Manage.* **2001**, *42*, 1349 – 1356.
[4] C. N. Hamelinck, A. P.. Faaij, *J. Power Sources* **2002**, *111*, 1 – 22.
[5] T. Chmielniak, M. Sciazko, *Appl. Energy* **2003**, *74*, 393 – 403.
[6] R. K. Grasselli, M. A. Tenhover, in *Handbook of Heterogeneous Catalysis* (Eds.: G. Ertl, H. Knözinger, F. Schüth, J. Weitkamp), Wiley-VCH, Weinheim, **2008**, pp. 3489 – 3517.
[7] S. Ilias, A. Bhan, *ACS Catal.* **2013**, *3*, 18 – 31.
[8] C. D. Chang, *Catal. Rev.* **1983**, *25*, 1 – 118.
[9] C. D. Chang, *Catal. Today* **1992**, *13*, 103 – 111.
[10] S. Yurchak, *Methane Conversion, Proceedings of a Symposium on the Production of Fuels and Chemicals from Natural Gas*, Elsevier, Amsterdam, **1988**.
[11] I. M. Dahl, S. Kolboe, *Catal. Lett.* **1993**, *20*, 329 – 336.
[12] I. Dahl, *J. Catal.* **1994**, *149*, 458 – 464.
[13] I. Dahl, *J. Catal.* **1996**, *161*, 304 – 309.
[14] H. Fu, W. Song, J. Haw, *Catal. Lett.* **2001**, *76*, 89 – 94.
[15] U. Olsbye, S. Svelle, M. Bjørgen, P. Beato, T. V. W. Janssens, F. Joensen, S. Bordiga, K. P. Lillerud, *Angew. Chem. Int. Ed.* **2012**, *51*, 5810 – 5831; *Angew. Chem.* **2012**, *124*, 5910 – 5933.
[16] C. Baerlocher, L. B. McCusker, *Atlas of Zeolite Framework Types*, Elsevier, Amsterdam, **2007**.
[17] U. Olsbye, S. Svelle, K. P. Lillerud, Z. H. Wei, Y. Y. Chen, J. F. Li, J. G. Wang, W. B. Fan, *Chem. Soc. Rev.* **2015**, *44*, 7155 – 7176.
[18] Q. Qian, J. Ruiz-Martínez, M. Mokhtar, A. M. Asiri, S. A. Al-Thabaiti, S. N. Basahel, B. M. Weckhuysen, *ChemCatChem* **2014**, *6*, 772 – 783.
[19] D. Mores, E. Stavitski, M. H. F. Kox, J. Kornatowski, U. Olsbye, B. M. Weckhuysen, *Chem. Eur. J.* **2008**, *14*, 11320 – 11327.
[20] D. Mores, J. Kornatowski, U. Olsbye, B. M. Weckhuysen, *Chem. Eur. J.* **2011**, *17*, 2874 – 2884.
[21] Q. Qian, J. Ruiz-Martínez, M. Mokhtar, A. M. Asiri, S. A. Al-Thabaiti, S. N. Basahel, B. M. Weckhuysen, *Catal. Today* **2014**, *226*, 14 – 24.
[22] M. Seiler, W. Wang, A. Buchholz, M. Hunger, *Catal. Lett.* **2003**, *88*, 187 – 191.
[23] V. Van Speybroeck, K. Hemelsoet, K. De Wispelaere, Q. Qian, J. Van der Mynsbrugge, B. De Sterck, B. M. Weckhuysen, M. Waroquier, *ChemCatChem* **2013**, *5*, 173 – 184.
[24] W. Song, H. Fu, J. F. Haw, *J. Am. Chem. Soc.* **2001**, *123*, 4749 – 4754.
[25] M. Bjørgen, F. Bonino, S. Kolboe, K.-P. Lillerud, A. Zecchina, S. Bordiga, *J. Am. Chem. Soc.* **2003**, *125*, 15863 – 15868.
[26] L. Palumbo, F. Bonino, P. Beato, M. Bjørgen, A. Zecchina, S. Bordiga, *J. Phys. Chem. C* **2008**, *112*, 9710 – 9716.
[27] J. L. White, *Catal. Sci. Technol.* **2011**, *1*, 1630.
[28] M. Bjørgen, S. Svelle, F. Joensen, J. Nerlov, S. Kolboe, F. Bonio, L. Palumbo, S. Bordiga, U. Olsbye, *J. Catal.* **2007**, *249*, 195 – 207.
[29] A. G. Gayubo, A. Alonso, B. Valle, A. T. Aguayo, J. Bilbao, *Appl. Catal. B* **2010**, *97*, 299 – 306.
[30] A. G. Gayubo, A. Alonso, B. Valle, A. T. Aguayo, J. Bilbao, *AIChE J.* **2012**, *58*, 526 – 537.
[31] J. Rass-Hansen, H. Falsig, B. Jørgensen, C. H. Christensen, *J. Chem. Technol. Biotechnol.* **2007**, *82*, 329 – 333.
[32] A. Morschbacker, *Polym. Rev.* **2009**, *49*, 79 – 84.
[33] A. P. Kagyrmanova, V. A. Chumachenko, V. N. Korotkikh, V. N. Kashkin, A. S. Noskov, *Chem. Eng. J.* **2011**, *176 – 177*, 188 – 194.
[34] V. F. Tret'yakov, Y. I. Makarfi, K. V. Tret'yakov, N. A. Frantsuzova, R. M. Talyshinskii, *Catal. Ind.* **2011**, *2*, 402 – 420.
[35] A. T. Aguayo, A. G. Gayubo, A. M. Tarrío, A. Atutxa, J. Bilbao, *J. Chem. Technol. Biotechnol.* **2002**, *77*, 211 – 216.
[36] E. Costa, A. Uguina, J. Aguado, P. J. Hernandez, *Ind. Eng. Chem. Process Des. Dev.* **1985**, *24*, 239 – 244.
[37] J. Schulz, F. Bandermann, *Chem. Eng. Technol.* **1994**, *17*, 179 – 186.
[38] R. Johansson, S. L. Hruby, J. Rass-Hansen, C. H. Christensen, *Catal. Lett.* **2009**, *127*, 1 – 6.
[39] D. Däumer, K. Räuchle, W. Reschetilowski, *ChemCatChem* **2012**, *4*, 802 – 814.
[40] J. P. Hofmann, D. Mores, L. R. Aramburo, S. Teketel, M. Rohnke, J. Janek, U. Olsbye, B. M. Weckhuysen, *Chem. Eur. J.* **2013**, *19*, 8533 – 8542.
[41] Q. Qian, J. Ruiz-Martinez, M. Mokhtar, A. M. Asiri, S. A. Al-Thabaiti, S. N. Basahel, H. van der Bij, B. M. Weckhuysen, *Chem. Eur. J.* **2013**, *19*, 11204 – 112015.
[42] K. Hemelsoet, Q. Qian, T. De Meyer, K. De Wispelaere, B. De Sterck, B. M. Weckhuysen, M. Waroquier, V. Van Speybroeck, *Chem. Eur. J.* **2013**, *19*, 16595 – 16606.
[43] E. Stavitski, M. H. F. Kox, B. M. Weckhuysen, *Chem. Eur. J.* **2007**, *13*, 7057 – 7065.
[44] R. Y. Brogaard, B. M. Weckhuysen, J. K. Nørskov, *J. Catal.* **2013**, *300*, 235 – 241.
[45] J. M. Grosselin, C. Mercier, G. Allmang, F. Grass, *Organometallics* **1991**, *10*, 2126 – 2133.

Received: August 9, 2015
Published online on October 14, 2015

